Progress In Electromagnetics Research M, Vol. 59, 111–121, 2017

Investigations of SAR Distributions and Temperature Elevation on Human Body at 60 GHz with Corrugated Antipodal Linear Tapered Slot Antenna

Purva Shrivastava[1] and T. Rama Rao[2, *]

Abstract—New generation wireless communications are expected to provide new services over the existing variety of wireless applications in the coming years. In this perspective, advances in utilization of computational electromagnetics (EM) and millimeter-waves (mmW) frequency bands make them as candidates for ultra-high-resolution and ultra-high-speed wireless communications. With the deployment of mmW wireless technologies, brinks of potential mmW induced biological and health effects should be evaluated carefully. The EM exposure is usually measured in terms of absorbed power from any user operating wireless devices. The exposure varies with the part of the body and location of the source that is exposed to the radio frequency waves. The purpose of this study is to observe EM exposure in terms of Specific Absorption Rate (SAR) and temperature elevations at mmWs from the designed Antipodal Linear Tapered Slot Antenna (ALTSA) at 60 GHz on different body parts utilizing EM computations and experiments with Infrared Thermal Camera.

1. INTRODUCTION

In recent years, progress in computational and millimeter wave (mmW) electronics has identified the mmW frequency band as highly promising for a number of ultra-high-resolution and ultra-high-speed short-range point-to-point and point-to-multipoint wireless communication applications [1, 2]. In addition to the large bandwidth, mmW enables integration of the whole transceiver inside a small chip due to the short wavelength (λ) of 10-1 mm [3, 4]. Integrated front-ends at 60 GHz are expected to be commercialized on wireless devices such as laptops, tablets, and headphones [4, 5], and mmW body centric communication systems are now under study [6]. Since the mmW radiation is absorbed by the Earth's atmosphere and has low thermal noise power levels [7], our generation is the first to become widely exposed to the mmW radiation.

However, at 60 GHz, path loss is more severe than at 2 or 5 GHz, and implementing a highly integrated transceiver in CMOS will be a challenging task [3]. As the path loss is high at 60 GHz, high antenna gain is required to compensate channel loss, and the maximum radiation should be directive towards the receiver [4]. Because mmW-based devices are high gain directional and adaptive antenna arrays [7,8], radiation energy is focused in certain directions, leading to increased power deposition in the main lobe points towards the human body. Also, mmW frequencies correspond to molecular sets containing carbon or oxygen molecular, and their interactions with human body are possible [9, 10]. Conventionally, horn, reflector and lens antennas have been used in mmW devices/systems. These antennas have high gain and efficiency but are not appropriate for low-cost commercial devices as they are bulky, costly, and heavyweight, and cannot be integrated with solid-state devices [4]. For these

Received 17 April 2017, Accepted 3 July 2017, Scheduled 11 August 2017

* Corresponding author: Thipparaju Rama Rao (ramaraotr@gmail.com).

[1] Department of Electrical Engineering, Tshwane University of Technology, Pretoria, South Africa. [2] RADMIC, Department of Telecommunication Engineering, SRM University, Chennai 603203, India.

reasons, the tapered slot antenna family based Antipodal Linear Tapered Slot Antenna (ALTSA) has been chosen as a strong candidate because of its compromise in terms of size and efficiency [11–13].

Recent research works have paid more attention to ALTSA for its prominent characteristics such as compact size, planar geometry, narrow beamwidth, high gain and wide bandwidth [12, 13]. ALTSA radiation at broadside improves link budget and reduces radiation towards the undesirable direction [4]. Recently, various antenna systems have been developed for mmW devices and tested for EM exposure compatibility. These systems are deficient with respect to the target exposure specifications because of the non-uniformity of the power density distribution at the surface of the subject, and have low exposure efficiency. Additional advantages of ALTSA are with respect to the target exposure specifications. The smooth pattern and high radiation efficiency help minimize trepidations due to the backscattering from biological tissues and enable desired uniform illumination of the surface, as the devices will be used close to human body which will result in near-field radiation. However, a conventional microstrip-like feeding system suffers from significant tradeoffs among cost, size and performance at microwave and mmW frequencies. The substrate integrated waveguide (SIW) technology inherits most of the advantages of complete shielding, low loss, ease of fabrication, high quality factor and high power-handling capability and is a promising technology for mmW systems [14, 15].

From the general public safety viewpoint, it is important to investigate the possible biological effects of low-power communication systems in the 60 GHz band before their wide, near-future deployment within domestic and professional environments, and very few studies are available on this topic [5, 9, 10, 16]. Various standardization bodies have defined the dosimetric quantities to measure the Radio Frequency (RF) exposure in the 10–300 GHz frequency range [17, 18]. It is found in the recent studies that power density is not very useful for assessing safety in near field as mmW devices will work near human body [19, 20]. Other dosimetric quantities such as Specific Absorption Rate (SAR) and temperature should be taken into account.

Usually, SAR is used to quantify the RF exposer for handheld devices [21, 22]. The SAR value varies with the part of the body and location of the source that is exposed to the RF energy. Unlike ultraviolet, X-ray, and gamma radiation, mmW radiation is non-ionizing and can produce non-mutagenic effects enflaming thermal energy in biological tissue that can be unsafe for human use [20]. Also due to the short wavelength and low penetration depth, energy absorption is confined to the skin surface, and it is difficult to evaluate a significant volume for SAR at mmWs. Thus, to conclude along with SAR values it is also important to obtain the temperature elevation in the human tissues. The SAR and temperature vary with the parts of the body and location of the source that is exposed to the electromagnetic (EM) radiation [20]. Therefore, for better understanding the interactions between the human body and antennas with a wireless device, such as a headphone, laptops and other wireless devises at the intended position, the antennas with wireless devices need to be characterized on skin-equivalent phantom models [16, 22, 23]. This paper focuses on the performance analysis of SAR distributions and temperature elevation for SIW based ALTSA using EM solver tool, Ansys's HFSS and experiments with Infrared Thermal Camera.

2. ANTENNA REQUIREMENTS, ARCHITECTURE AND DESIGN

2.1. Antenna Model

The requirements of the antenna for the wireless devices are dictated by five parameters: dimension, resonant frequencies, bandwidth, radiation efficiency and SAR [21]. With the reduction in the overall size of modern wireless devices and the increasing number of supported systems, the antennas size has been squeezed into an ever reducing space. The size of the proposed ALTSA is very compact, i.e., $43.29 \times 9.93 \times 0.381\,\text{mm}^3$ and is designed on a 0.381 mm RT/Duroid 5880 substrate with dielectric permittivity $\varepsilon_r = 2.20$ and $\tan\delta = 0.0004$. On one side, the input track is flared to produce half of the linear TSA, and the ground plane is flared in the opposite direction to form the overall balanced antipodal. The center frequency of ALTSA is 60 GHz, and the length of tapered slot line is 4.5λ. One of the advantages of the antipodal geometry is that it does not need to layout any stubs on the printed circuit board to achieve impedance matching. Flares are designed to overlap each other to avoid the mismatch as input impedance of the ALTSA is high and that of the SIW is low.

The SIW feeding structure has two periodic rows of metalized cylindrical vias connecting the upper and lower flares of ALTSA which acts as dielectric filled rectangular waveguide. Diameter of a via and the space between the vias should be measured precisely to ensure loss free radiation between the metallic vias because of diffraction. On small antennas, undesired surface current on the outline leads to near-field radiation and thereby leads to reduced gain as well as high side lobe levels (SLL) [12, 13]. A planar corrugated surface of exactly $\lambda/4$ resonant depth blocks the propagation of an oblique plane wave whose wave vector is perpendicular to the corrugation independently from the direction of the electric field, thus helping them to minimize the radiation toward the undesired direction [12, 13]. Outer rectangular corrugation structures are applied to the ALTSA design. The length and width dimensions of the corrugation module are $\lambda/4$ and $\lambda/10$, respectively. Fig. 1 depicts a prototype version of the proposed ALTSA with outer rectangular corrugation.

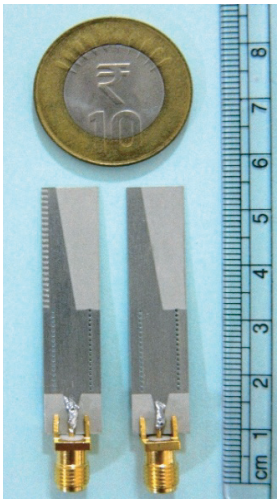

Figure 1. Photograph of fabricated corrugated ALTSA.

2.2. Antenna Performance

The performance measurements are carried out utilizing Vector Network Analyzer [24, 25] and calibrated with single port to test the return loss at 60 GHz and record the radiation pattern. The separation between the antennas is maintained to be greater than the far-field requirement [13, 24, 25]. The antenna patterns in E-plane and H-plane are observed, and the measured gain of the antenna is 16.5 dB. Figs. 2 and 3 depict radiation patterns and the far-field pattern for both E and H planes. It is observed that the main lobe is in the substrate plane (y-axis). This is significant, since mmW application needs a good stability of radiation pattern and directivity.

The 3 dB beamwidth is 34.6° while the SLL is −9 dB. The radiation efficiency of the corrugated ALTSA is 96.84%. The performance summary and comparison of the proposed corrugated ALTSA with other similar works available in the literature are shown in the Table 1.

Table 1. Performance summary and comparison of the proposed ALTSA with other similar works.

References	Frequency (GHz)	Size (mm)	Gain (dB)	Beamwidth (°)
Proposed ALTSA	60	22.35	16.4	34.6
[26] (2012)	28	25.6	12.2	48
[27] (2013)	41–61	45	14.9	$33 \approx 36$
[28] (2013)	35	27.1	14.5	15
[29] (2014)	50–70	17.5	14.7 ± 0.5	25

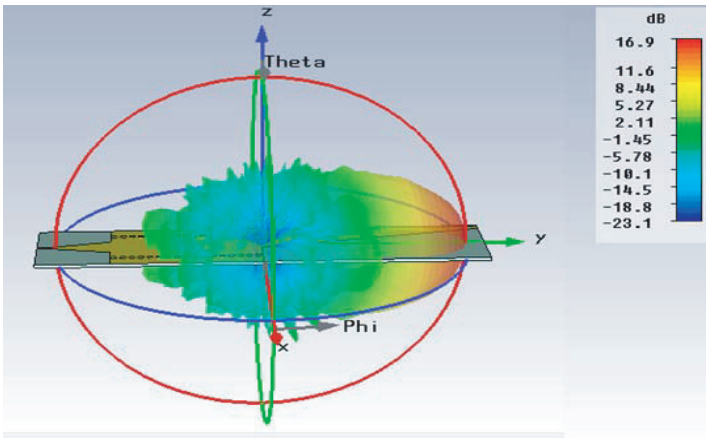

Figure 2. Radiation pattern of corrugated ALTSA.

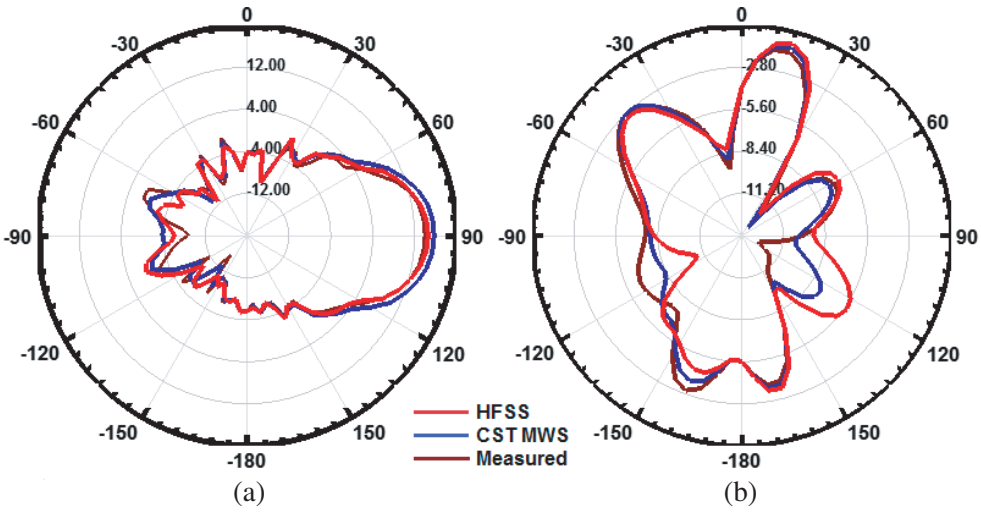

Figure 3. E and H plane pattern of corrugated Antipodal Linear Tapered Slot Antenna.

3. INTERACTION AND EFFECT OF EM WAVES

3.1. Dielectric Properties

EM fields depend not only on the strength and frequency of the external fields because of several dispersion mechanisms affecting human tissues, but also on the shape, size and electrical characteristics of the body and the orientation of the body in relation to the external fields [21–23]. EM field and its biological effects depend on the energy absorbed and the ability to heat human tissues. To explore the reflection transmission and absorption properties of the body, knowledge of the dielectric properties of the body tissue is essential. The electrical permittivity and conductivity are important properties to evaluate the EM and power distribution in the body as the magnetic permeability of body tissues is equivalent to the free space [9]. The tissue properties at 60 GHz chosen according to the database developed [20, 30] and the thicknesses of tissues are given in Table 2 and Table 3.

3.2. Absorption in Human Body

As the human tissues are transparent to RF fields, when the body is exposed near the device, the RF fields penetrate the human tissues. The depth of penetration depends on the frequency and conductivity of the tissues. As the conductivity varies with human tissues at different frequencies, different kinds of tissues should be taken into consideration.

Table 2. The dielectric properties of the biological tissues at 60 GHz.

Tissues	σ **(S/m)**	$\varepsilon_{\mathbf{r}}$	$\tan\delta$	**Penetration depth [mm]**
Skin	36.38	7.98	1.37	0.48
Fat	2.81	3.13	0.27	3.37
Muscle	52.82	12.86	1.23	0.41
Bone	7.20	3.81	0.57	1.49

Table 3. Thickness of the biological tissues.

Tissues	Head [mm]	Anterior Thighs [mm]
Skin	1.5	1.92
Fat	7	7.65
Muscle	31	31
Bone	31	31

3.3. Body Model

In order to reasonably predict the effects of the human body on the propagation and absorption of mmW signals, accurate tissue models for mmW propagation prediction need to be developed. Personal wireless devices are operated close to the head and body, which means that normally 10–90% of the transmit power is absorbed into the user. The generated internal fields depend not only on the strength and frequency of the external fields, but also on the anatomy, orientation distance from the radiator and electrical characteristics of the body. When creating the models for the simulations, the idea is to keep an industrial point of view. Thus a four-layer human body homogeneous model with external shapes and sizes consisting of skin, fat, muscle and bone has been used.

The 3D human tissue models representing two body parts, head and anterior thighs, are used for the study of SAR. Model 1 simulates the tissue layers structure of head, along with headphone, and model 2 represents the tissue structure of the anterior thighs along with laptop. To limit the simulation time, some of the smaller parts are left out during simulations. Further, wireless devices and the applicator are set under perfectly conducting materials. The casing and glass top of the laptop display are set as lossless dielectric materials, and the rest of the parts are set as perfectly conducting materials. The absorption is affected by the distance from the radiator, the anatomy and orientation of the user and the electrical characteristics of the tissues. The SAR is evaluated at 60 GHz with 1, 10 and 100 mW transmitting power same as that assigned by IEEE Standard 802.15.3-2003 to enable wireless connectivity of high-speed, low-power, low-cost, multimedia-capable portable electronic devices [32].

3.4. Dosimetric Quantities to Measure RF Exposure

Dosimetric quantities have been established by various standardization bodies [17, 18] to determine exposure compliance. The three major dosimetric quantities commonly studied are:

(i) Power Density (PD): PD is adopted as one of the main exposure characteristics by most of the international guidelines and standards in the 10–300 GHz frequency range.

(ii) Specific absorption rate (SAR): The SAR distribution can be easily estimated with the electric field distribution inside the tissue. The area with maximum EM field corresponds to the region with maximum SAR value.

(iii) Steady-state and/or transient temperature (T): Heating effects can be hazardous if exposure is sufficiently intense or prolonged leading to localized temperature elevation, thus along with the PD and SAR the study of heating is useful to protect humans.

4. SPECIFIC ABSORPTION RATE AT MILLIMETER WAVES

The dosimetric quantity used in the international organizations guidelines for frequencies above 6 GHz is PD [17, 18]. However, it is important to note that the current recommendations do not provide any recommendations for near-field exposures and only deal with far-field exposures at mmW. Due to the limited practical studies and interests at millimeter waves in the past, these guidelines do not really provide a dosimetric quantity or methodology for this type of near-field exposures. Evaluations based on PD depends only on the density of power traveling toward the tissues and do not rely on knowledge of the distribution of fields or power absorption in the tissues, unlike evaluations of SAR or temperature [19, 20]. Hence, PD is not as useful as SAR or temperature for evaluating safety in mmW devices, especially in the near field. In several studies, SAR has been used as one of the dosimetric quantities at millimeter waves to study the exposure [9, 19, 31].

The spatial SAR distributions in homogeneous phantom models due to ALTSA are computed at 60 GHz using Ansys's HFSS. The total computing time is about a week, and the computing platform is Intel Core i7 with 124 GB RAM. The results demonstrate that ALTSA has only slight impact on the human body proximity at 60 GHz, and the influence of the human body is very weak. The antenna return loss remains below −10 dB at 60 GHz on the tissue-equivalent model. It can be seen that radiations remain very slightly affected in the E-plane and H-plane due to the absorption and reflection. The antenna efficiency is found stable at 60 GHz. Fig. 4 illustrates the SAR on layered tissue human head model with headphone. The second cases are taken into consideration as the thickness of the tissues varies according to different parts of the body. Fig. 5 illustrates the SAR on Anterior Thighs with laptop.

Table 4 depicts the SAR values for the two scenarios. From the results it is found that at 60 GHz the skin depth of radiation lessens, causing the currents to conduit near the surface of the body creating hotspots. However, at 60 GHz, the significance of the hotspots around the source decreases due to the

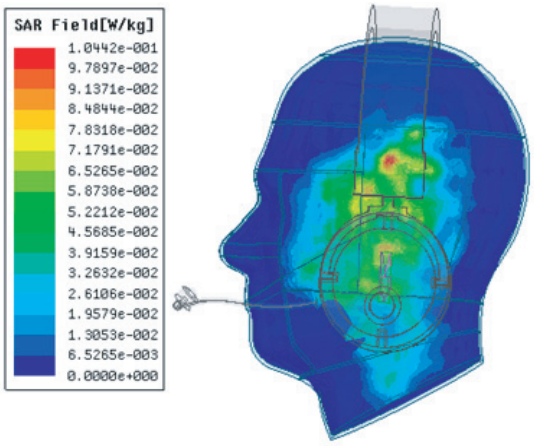

Figure 4. SAR on human head with headphone at 10 mW for 1 gram of tissue.

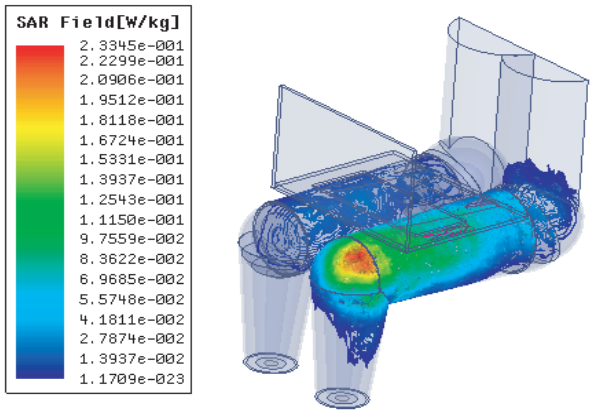

Figure 5. SAR on Anterior Thighs with laptop at 10 mW for 1 gram of tissue.

Table 4. SAR values for two scenarios at 60 GHz.

Anatomical site	**1 gram of tissue SAR(W/kg)**		
	Transmitting Power (mW)		
	1 mW	10 mw	100 mW
Head	$1.0442e^{-002}$	$1.0442e^{-001}$	1.0442
Anterior Thigh	$2.3345\ e^{-002}$	$2.3345\ e^{-001}$	2.3342

strong attenuation of the fields in tissues. In addition to the electrical requirements, the design of a wireless device has to take into account. However, the studies also show that the distance between the body and the wireless device affects the behavior of SAR. ALTSA is kept at a distance of 5 mm from body. The SAR obtained for both laptop and headphone model is way lower than the normative limits set for the antenna designer which is 1.6 W/kg for partial body (head) exposure and 4 W/kg for exposure to the hands, wrists, feet and ankles [17, 18, 37]. The resulting SAR values of wireless devices are greatly affected by the applied transmitting power level. With the maximum transmitted power of 100 mW, the SAR is increased to 100 folds. Comparisons of the ALTSA SAR values with other works available in the literature are given in Table 5. It is found that the SAR values due to ALTSA are way lower than the reported values at 60 GHz and lower frequencies.

Table 5. Comparisons of the SAR results with other literature.

Ref.	Frequency GHz	Antenna	Method	Anatomical site	SAR	Power (mW)	Distance (mm)
	60	ALTSA	FEM	Head	1.0442 W/kg	100	5
				Anterior Thigh	2.3342 W/kg		
[16]	60	Patch array	FDTD	Body	165.6 W/kg	322	5.6
[36]	60	Open Ended Waveguide	FDTD	Hand	3010 W/kg	500	15
[38]	60	Microstrip Patch antenna	FDTD	Body	279 W/kg	1 W	1
[33]	2.4	PIFA	FDTD	Torso	0.399 mW/kg	100	34
				Head	0.057 mW/kg		
[34]	13.56 MHz	Coil Antenna	FDTD	Hand	6.52 mW/kg	100	-
				Ear	0.26 mW/kg		-
				Chest	1.52 mW/kg		20
				Hip	11.18 mW/kg		5
[35]	2.4 GHz	Monopole and PIFA	FDTD	Head	3.56 W/kg PIFA	100	7
					3.86 W/kg Mon-opole		5.32
				Ear	0.49 W/kg PIFA		39.87
[36]	60 GHz	WR-15 open-ended rectangular waveguide	FDTD	Hand	2.97 kW/kg	500	15

5. MILLIMETER WAVE HEATING OF THE SKIN

The temperature rise in head and anterior thigh models due to ALTSA is computed at 60 GHz using Ansys's HFSS. In the experimental setup, the subjects are exposed to 60 GHz using an ALTSA applicator connected to WR-51 adapter located on the body with wireless devices based models. To generate 60 GHz frequency, a reference signal of 10 MHz and an intermediate frequency of 3 GHz are fed to the 60 GHz transceiver through a signal generator (Keysight's N5182A MXG). 10 mW of input power is fed in regards to the limitation consistent with regulatory arrangement for unlicensed transceiver

devices in the 57–64 GHz band. FLIR A305sc Infrared Thermal Camera is used to measure the temperature elevation operating in the 7.5–14 μm spectral range, and its thermal sensitivity is 0.05°C. FLIR A305sc is connected to FLIR Tools+ to display the live image stream. Repeated measurements are performed on the head and anterior thighs. Data and images are collected for every 30 minutes of operation/experiment.

With 10 mW incident power, it is observed that the maximum temperature elevation on the skin surface during simulation and measurement is about 0.82° and 0.6°, respectively, which is below the temperature threshold of 1° according to IEEE standards on mmW radiation guidelines [19, 20]. Figs. 6(a) and (b) illustrate the simulated temperature distributions at 60 GHz for head and anterior thighs. From the results it is illustrated that due to high directivity of ALTSA, more current is conducted on the surface of the body along the main lobe direction, creating hotspots. The hotspot in the

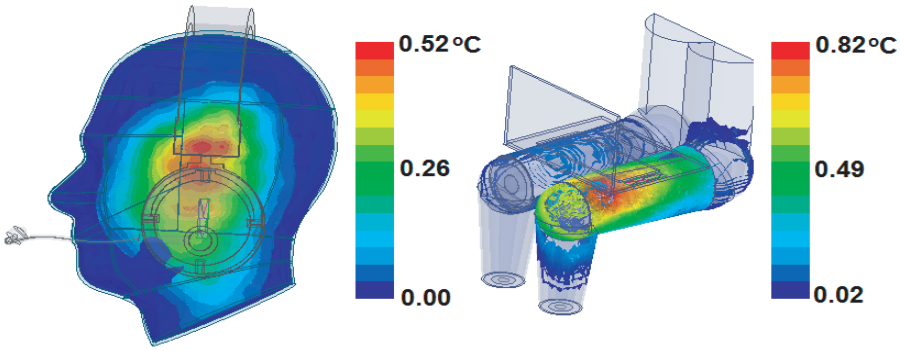

(a) (b)

Figure 6. Temperature distribution. (a) Head model. (b) Anterior thighs model.

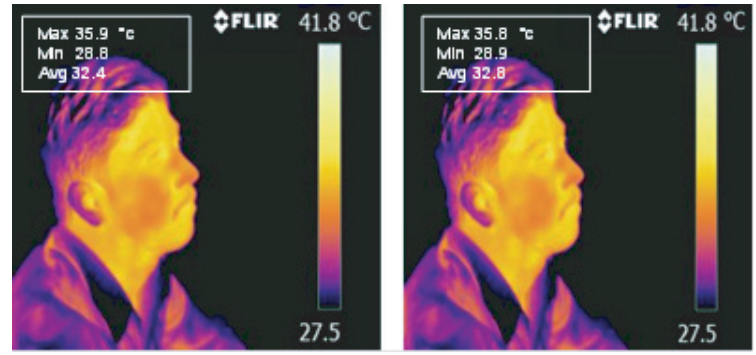

(a)

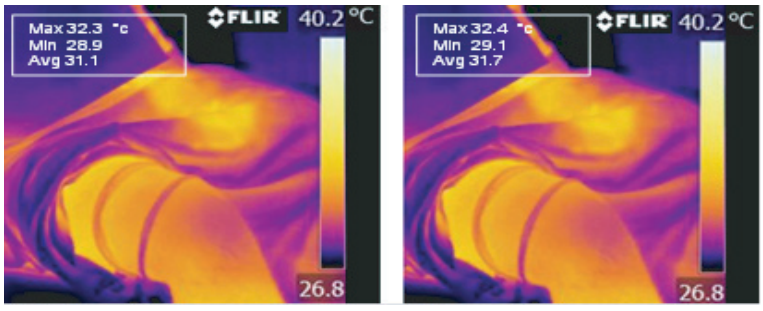

(b)

Figure 7. Heat distribution before and after the exposure for 30 minutes. (a) Head. (b) Anterior thighs.

figures represents the location of the maximum temperature. Figs. 7(a) and (b) illustrate the thermal distributions on head and anterior thighs before and after the exposure of 30 minutes. Fig. 8 shows the steady state temperature rise at 60 GHz for head and anterior thighs. In both the cases during simulation and measurement, maximum temperature value appears around 1000 seconds in the transient curve. All the graphs have a steady state, when the maximum rise of temperature is approached, and the rise of temperature is constant in function of time. In thighs and head, thermal elevation is high since the skin is covered completely with laptop and headphone, and it does not allow thermal conduction. Simulated and measured maximum temperature rises for both the scenarios are given in Table 6.

Table 6. Maximum Temperature Rise at 60 GHz.

Model	Maximum Temperature [°C]	
	Simulated	Measured
Head	0.52	0.4
Anterior Thighs	0.82	0.6

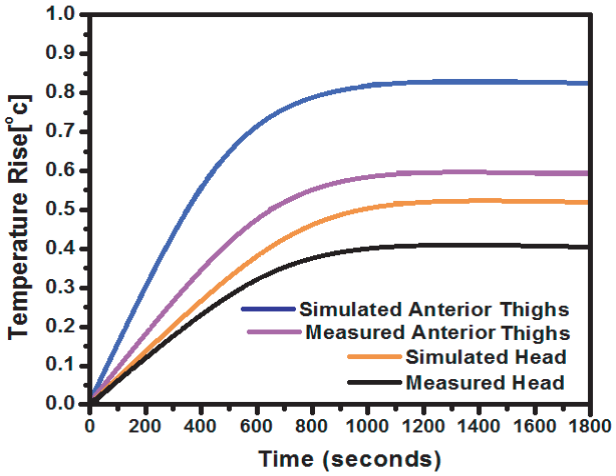

Figure 8. Time evolution of increase of temperature in head and anterior thighs.

6. CONCLUSIONS

For the new generation wireless device applications at mmWs, SAR distribution and temperature elevation analysis are performed on a multi-layered human tissue model using SIW-based ALTSA at 60 GHz. The temperature rises on head and anterior thighs due to ALTSA are computed at 60 GHz using Ansys's HFSS. Thermal elevation measurements are performed using FLIR A305sc Infrared Thermal Camera, and EM simulations are conducted utilizing tissue layered model. It is observed that both SAR and temperature elevation depend not only on the applied power and frequency of operation, but also on the shape, size and electrical characteristics of the body tissues. The values obtained for SAR and temperature elevation in both the cases are below the safety level given in the IEEE standard. It makes the SIW-based ALTSA a reliable candidate for the wireless devices which will flourish very widely for variety of wireless applications.

ACKNOWLEDGMENT

The authors are very much grateful to the DRDO, Government of India for their great support in executing this research work.

REFERENCES

1. Celik, N., M. F. Iskander, R. Emrick, S. J. Franson, and J. Holmes, "Implementation and experimental verification of a smart antenna system operating at 60 GHz band," *IEEE Trans. Antennas Propag.*, Vol. 56, No. 9, 2790–2800, Sep. 2008.
2. Baykas, T., C. S. Sum, Z. Lan, J. Wang, M. A. Rahman, and H. Harada, "IEEE 802.15.3c: the first IEEE wireless standard for data rates over 1 Gb/s," *IEEE Communications Mag.*, Vol. 49, No. 7, 114–121, Jul. 2011.
3. Jiang, C., "Microwave and millimetre wave integrated circuit system in packaging," DTU Electrical Engineering, Technical University of Denmark, Jan. 2010.
4. Huang, K. C. and D. J. Edwards, *Millimetre Wave Antennas for Gigabit Wireless Communications*, 1st Edition, John Wiley, Chichester, 2008.
5. Cotton, S. L., W. G. Scanlon, and B. K. Madahar, "Millimeter-wave soldier-to-soldier communications for covert battlefield operations," *IEEE Communications Mag.*, Vol. 47, No. 10, 72–81, Oct. 2009.
6. Chahat, N., M. Zhadobov, and R. Sauleau, "Wearable end-fire textile antenna for on-body communications at 60 GHz," *IEEE Antennas Wirel. Propag. Letters*, Vol. 11, 799–802, Jul. 2012.
7. Yong, S. K. and C. C. Chong, "An overview of multi gigabit wireless through millimeter wave technology: Potentials and technical challenges," *EURASIP Journal on Wireless Communications and Networking*, Article ID 78907, 2007.
8. Gutierrez, F., S. Agarwal, K. Parrish, and T. S. Rappaport, "On chip integrated antenna structures in CMOS for 60 GHz WPAN systems," *IEEE J. Sel. Areas Commun.*, Vol. 27, No. 8, 1367–1378, Oct. 2009.
9. Zhadobov, M., N. Chahat, R. Sauleau, C. L. Quement, and Y. Le drean, "Millimeter-wave interactions with the human body: State of knowledge and recent advances," *Int. Journal of Microwave and Wirel. Tech.*, Vol. 3, No. 2, 237–247, Apr. 2011.
10. Gandhi, O. P. and A. Riazi, "Absorption of millimeter waves by human beings and its biological implications," *IEEE Trans. Microwave. Theory Tech.*, Vol. 34, No. 2, 228–235, Feb. 1986.
11. Coburn, W. K. and A. I. Zaghloul, "Numerical analysis of stacked tapered slot antennas," *28th Annual Review of Prog. in Applied Comput. Electromagt.*, 112–117, Ohio, 2012.
12. Shrivastava, P., D. Chandra, N. Tiwari, and T. Rama Rao, "Investigations on corrugation issues in SIW based antipodal linear tapered slot antenna for wireless networks at 60 GHz," *Applied Computational. Electromagnetics Society Journal, ACES*, Vol. 28, No. 10, 960–96, Oct. 2013.
13. Shrivastava, P. and T. Rama Rao, "60 GHz radio link characteristic studies in hallway environment using antipodal linear tapered slot antenna," *IET Microwaves, Antennas & Propagation*, Vol. 9, No. 15, 1793–1802, 2015.
14. Bozzi, M., L. Perregrini, K. Wu, and P. Arcioni, "Current and future research trends in substrate integrated waveguide technology," *Radioengineering*, Vol. 18, No. 2, 201–20, 2009.
15. Zhang, Y., W. Hong, and Z. Kuai, "A SIW fed antipodal linear tapered slot planar multi-beam antenna for millimeter-wave application," *Journal of Electromagnetic Engineering and Science*, Vol. 10, No. 3, 175–178, 2010.
16. Chahat, N., M. Zhadobov, L. Le Coq, S. Alekseev, and R. Sauleau, "Characterization of the interactions between a 60-GHz antenna and the human body in an off-body scenario," *IEEE Trans. Antennas Propag.*, Vol. 60, No. 12, 5958–5965, Dec. 2012.
17. IEEE Standards Interpretations for IEEE Std C95.1^{TM}-2005 "IEEE Standard for Safety Levels with Respect to Human Exposure to Radio Frequency Electromagnetic Fields, 3 kHz to 300 GHz".
18. International Commission on Non-Ionizing Radiation Protection (ICNIRP), "Guidelines for limiting exposure to time-varying electric, magnetic, and electromagnetic fields (up to 300 GHz)," *Health Physics*, Vol. 74, No. 4, 494–522, Apr. 1998.
19. Wu, T., T. S. Rappaport, and C. M. Collins, "Safe for generations to come: Considerations of safety for millimeter waves in wireless communications," *IEEE Microwave Mag.*, Vol. 16, No. 2, 65–84, Mar. 2015.

20. Wu, T., T. S. Rappaport, and C. M. Collins, "The human body and millimeter-wave wireless communication systems: Interactions and implications," *IEEE International Conference on Communications (ICC)*, Jun. 2015.
21. Halla, P., "Specific absorption rate design of 3rd generation handsets," Mater Dissertation Theses, Helsinki University Of Technology, Finland, 2008.
22. Butet, R., Y. Toutain, S. L. Dall, J. Luc, L. J. Foged, and J. Estrada, "A fast SAR measurements system for production testing of personal wireless devices," *IEEE Intern. Symp. on Antennas and Prop. Society (APSURSI)*, 2026–2027, Jul. 2013.
23. Alekseev, S. I. and M. C. Ziskin, "Human skin permittivity determined by millimeter wave reflection measurements," *Bioelectromagnetics*, Vol. 28, No. 5, 331–339, 2007.
24. http://www.abmillimetre.com/Introduction.html.
25. Millimetre, A. B., "An 8 to 1000 GHz vector network analyser," *Microwave Journal*, Vol. 35, No. 3, Mar. 1992.
26. Djerafi, T. and K. Wu, "Corrugated Substrate Integrated Waveguide (SIW) antipodal linearly tapered slot antenna array fed by quasi-triangular power divider," *Progress In Electromagnetics Research C*, Vol. 26, 139–151, 2012.
27. Taringou, F., D. Dousset, J. Bornemann, and K. Wu, "Broadband CPW feed for millimeter-wave SIW-based antipodal linearly tapered slot antennas," *IEEE Trans. Antennas Propag.*, Vol. 61, No. 4, 1756–1762, 2013.
28. Wang, W., X. Wang, W. Wang, and A. E. Fathy, "Planar high-gain antipodal linearly tapered slot antenna for passive millimeter-wave focal plane array imaging," *Proc. IEEE Int. Symp. Phased Array Systems & Tech.*, 267–271, Waltham, MA, USA, Oct. 2013,
29. Ismail, M. and A. R. Sebak, "High-gain SIW-based antipodal linearly tapered slot antenna for 60-GHz applications," *Proc. IEEE Antennas Prop. Society Int. Symp.*, 217–218, Memphis, Tennessee, USA, Jun. 2014.
30. Italian National Research Council, Institute for Applied Physics, Florence, Italy, "Dielectric properties of body tissue in the frequency range 10 Hz–100 GHz," www-page, available at http://niremf.ifac.cnr.it/tissprop/, cited 15.09.2007.
31. Alekseev, S. I., et al., "Millimeter wave dosimetry of human skin," *Bioelectromagnetics*, Vol. 29, No. 1, 65–70, 2008.
32. Gilb, P. K. J., "Wireless multimedia: A guide to the IEEE 802.15. 3 standard," IEEE Standards Association, 2004.
33. Findla, R. P. and P. J. Dimbylow, "SAR in children from exposure to Wireless Local Area Networks (WLAN)," *Proc. Symposium on Asia Pacific Electromagnetic Compatibility*, 733–736, Singapore, May 2012.
34. Cecil, S., G. Schmid, K. Lamedschwandner, J. Morak, G. Schreier, A. Oberleitner, and M. Bammer, "Numerical assessment of specific absorption rate in the human body caused by NFC devices," *IEEE Second International Workshop on Near-field Communication (NFC)*, 65–70, Monaco, Apr. 2010.
35. Pizarro, Y. A. A., A. A. de Salles, S. Severo, J. L. T. Garzon, and S. M. R. Bueno, "Specific Absorption Rate (SAR) in the head of Google glasses and Bluetooth user's," *IEEE Latin-America Conference on Communications (LATINCOM)*, 1–6, Cartagena, Colombia, Nov. 2014.
36. Chahat, N., M. Zhadobov, and R. Sauleau, "Broadband tissue-equivalent phantom for BAN applications at millimeter waves," *IEEE Trans. on Microwave Theory Tech.*, Vol. 60, No. 7, 2259–2266, 2012.
37. Evaluating Compliance with FCC Guidelines for Human Exposure to Radiofrequency Electromagnetic Fields, Federal Communications Commission Standard, OFT Bulletin 65, Edition 97-01.
38. Chahat, N., M. Zhadobov, and R. Sauleau, "Antennas for body centric wireless communications at millimeter wave frequencies," *Progress in Compact Antennas*, InTech, 2014.